Human Sensory-Musculoskeletal Modeling and Control of Whole-Body Movements

Chenhui Zuo* **Guohao Lin*** **Chen Zhang*** **Shanning Zhuang** **Yanan Sui†**

Tsinghua University

Abstract

Coordinated human movement depends on the integration of multisensory inputs, sensorimotor transformation, and motor execution, as well as sensory feedback resulting from body-environment interaction. Building dynamic models of the sensory-musculoskeletal system is essential for understanding movement control and investigating human behaviors. Here, we report a human sensory-musculoskeletal model, termed SMS-Human, that integrates precise anatomical representations of bones, joints, and muscle-tendon units with multimodal sensory inputs involving visual, vestibular, proprioceptive, and tactile components. A stage-wise hierarchical deep reinforcement learning framework was developed to address the inherent challenges of high-dimensional control in musculoskeletal systems with integrated multisensory information. Using this framework, we demonstrated the simulation of three representative movement tasks, including bipedal locomotion, vision-guided object manipulation, and human-machine interaction during bicycling. Our results showed a close resemblance between natural and simulated human motor behaviors. The simulation also revealed musculoskeletal dynamics that could not be directly measured. This work sheds deeper insights into the sensorimotor dynamics of human movements, facilitates quantitative understanding of human behaviors in interactive contexts, and informs the design of systems with embodied intelligence.

Introduction

Humans interact with the external world through coordinated body movements enabled by the interplay of the sensory, musculoskeletal, and central nervous systems. These systems orchestrate multisensory integration, sensorimotor transformation, and motor execution in a closed-loop manner. Developing a comprehensive, controllable whole-body model of the human sensory-musculoskeletal system is crucial for analyzing motor control and designing embodied intelligence.

Modeling the human sensory-musculoskeletal system requires detailed anatomical and biomechanical representations, along with sensorimotor control. The adult human musculoskeletal system comprises approximately 206 bones, over 200 joints, and more than 600 skeletal muscles[1]. Previous musculoskeletal models typically focused on specific body parts[2, 3, 4, 5, 6]. Some models allowed whole-body simulation but with simplified muscle construction to ease the control process[7, 8]. While offering insights into joint mechanics and muscle forces, these often simplified muscle structures or lacked sensory components, limiting whole-body coordination. Beyond biomechanics, sensory feedback is vital for adaptive motor control. Proprioceptive, tactile, vestibular, and visual

*These authors contributed equally to this work.

†Corresponding author, ysui@tsinghua.edu.cn

39th Conference on Neural Information Processing Systems (NeurIPS 2025) Workshop: Foundation Models for the Brain and Body.

systems provide critical information for body state, balance, and spatial awareness. Integrating these modalities is fundamental for dynamic stability and complex task coordination.

The inherent complexity of the sensory-musculoskeletal system poses significant computational challenges, including nonlinear muscle dynamics, multi-joint coordination, ultra-high dimensionality of muscle actuation space, and dynamic adaptation to environmental changes.

To overcome these challenges, we developed a sensory-musculoskeletal human model, termed SMS-Human, that integrates the whole-body musculoskeletal system with multiple sensory components. This model achieves comprehensive anatomical representation that comprises 175 rigid body segments with 206 precise bone meshes, 278 joints, and 1,266 muscle-tendon units, with accurate spatial and validated functional parameters. We incorporated multimodal sensory (binocular visual, vestibular, proprioceptive, and tactile) inputs (Fig. 1a-f) in our simulation with the open-source MuJoCo physics engine [9].

We developed a hierarchical deep reinforcement learning (DRL) approach with efficient representations of high-dimensional actuators and a stage-wise learning process for training a neural network controller that could simulate human motor behaviors using the SMS-Human model. We demonstrated successful control of coordinated human-like movements with high physiological and behavioral fidelity, including bipedal locomotion, vision-guided object manipulation, and bicycling. The unprecedented anatomical detail of our model provides a new foundation for computational analysis of human sensory-musculoskeletal system in a closed-loop, physics-based way, and for studying spatiotemporal dynamics for whole-body movement control.

Sensory-Musculoskeletal Modeling and Control

The SMS-Human model integrates multimodal sensory inputs to enable sensorimotor transformation for motor behaviors in the simulation environment (Fig. 1). Binocular sensing was implemented via the cameras positioned in the eyes, providing the egocentric view of the model during the task performance (Fig. 1a, b). The vestibular system was provided by sensors located in the head, measuring the linear and rotational head motion and orientation important for maintaining balance and coordinating eye-head movements (Fig. 1c). Proprioceptive components encoded the angular position (P), velocity (V), and acceleration (A) for all joints, as well as the length (L), velocity (V), force (F), and activation (Act) for all muscle-tendon units (Fig. 1d). This comprehensive proprioceptive information on the joints and muscle-tendon units allows precise control of posture and movement. We placed touch sensors for measuring contact forces over the body, as shown by the forces detected at the hands (Fig. 1e) and feet (Fig. 1f). This tactile feedback is important for the model to execute stable bipedal locomotion and fine motor tasks such as object manipulation.

Each modality of sensory input was represented by corresponding matrices shown in Fig. 1j. A neural network controller was trained to generate motor output in the action space based on multisensory input, as represented by the motor actuation matrix (Fig. 1k). The learned motor actions served as neural excitation to actuate skeletal muscles for motor behaviors in response to the observed state (Fig. 1h,i). Both the state and action spaces were high-dimensional in nature (Fig. 1j,k and Extended Data Table 1). This scheme of integrating biomechanical model with multimodal sensing represents the basis for the embodied simulation.

Construction of embodied human sensory-musculoskeletal model

We decomposed anatomical structures of the human musculoskeletal system into functional units. The 206 bones were grouped into 175 rigid body segments capable of independent movement and connected by 278 joints. Human skeletal muscles were implemented as 1,266 muscle-tendon units. Muscles with broad attachment positions were modeled using multiple muscle-tendon units, which resulted in a greater number of muscle-tendon units than the anatomical counts. We constructed the skeleton for a typical adult male through selective integration of existing databases and models[2, 3, 5, 10, 11], with further refinement based on published anatomical data. The body segment-specific dynamic parameters included mass and inertial properties, which were calculated by estimating segment volume and tissue density.

The body segments were articulated through joints, whose position, axis orientation, range of motion (ROM), and kinematic coupling were explicitly parameterized within the model. We determined

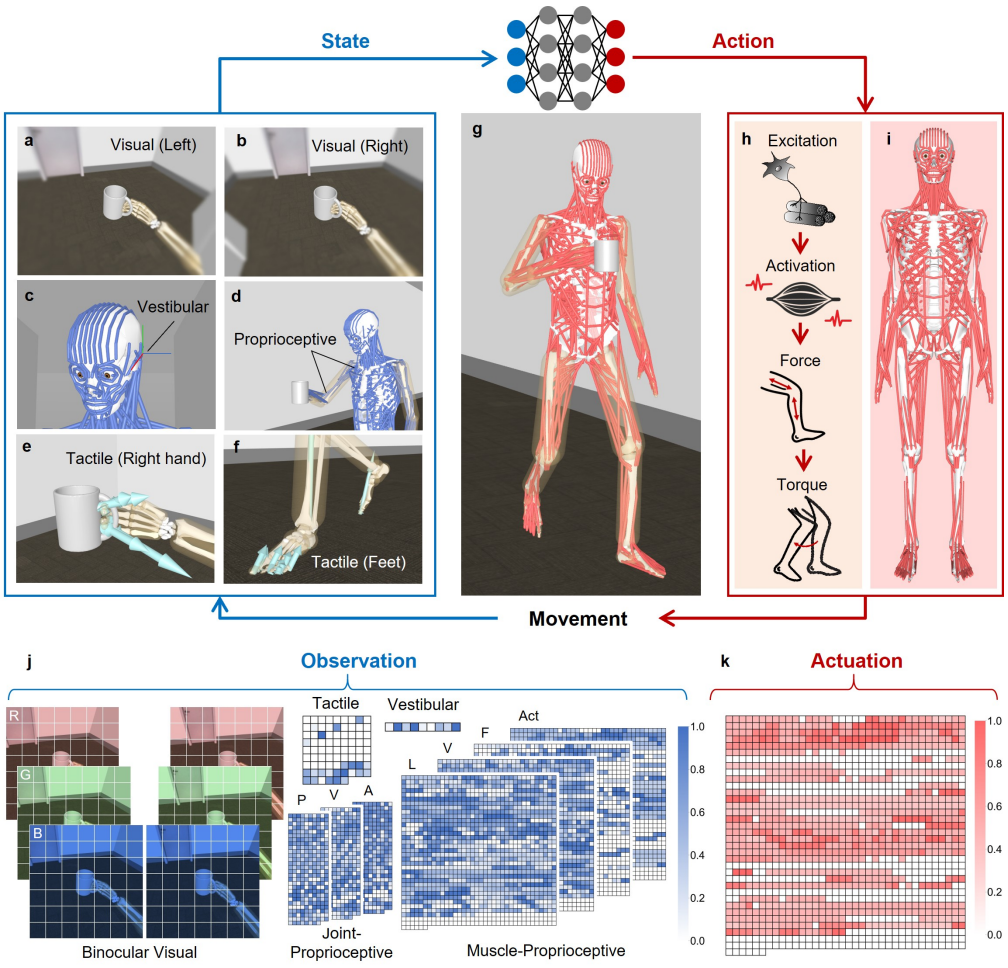

Figure 1: **Human sensory-musculoskeletal model with sensorimotor transformation and feedback control**. **a,b**, Binocular inputs provided by cameras in the left eye (**a**) and right eye (**b**), with progressive peripheral blurring to simulate human foveal vision. **c**, Vestibular information provided by sensors located in the head. **d**, Proprioceptive inputs provided by sensors in joints and muscle-tendon units. **e,f**, Tactile inputs in hands (**e**) and feet (**f**), with light blue arrows indicating contact forces. **g**, Full-body visualization of SMS-Human during walking, while looking at the mug in the hand. **h**, Neural control pathway for movement generation, including neural excitation, muscle activation, force and torque generation. **i**, Musculoskeletal representation of SMS-Human model, featuring 1,266 muscle-tendon units (red lines) to actuate the whole-body skeleton. **j**, High-dimensional inputs to the DRL network at a single time point, including binocular images at RGB channels (224x224x3x2), conjugated vestibular inputs (9x1), tactile inputs (78x1), joint proprioceptive inputs (278x3), and muscular proprioceptive inputs (1266x4). Separate matrices for position (P), velocity (V), acceleration (A), length (L), force (F), and activation (Act) are shown for proprioceptive components. Color intensity represents the normalized value for all modalities except vision (represented in RGB space). **k**, Motor activation in the action space (1266x1). Color intensity represents activation level. In **a–g**, translucent yellow capsules surrounding skeletal structures represent the body-environment interface modeling.

the joint configurations by detailed examination of data from original human anatomical studies[12, 13, 14, 15, 16, 17] and previous simulation models[2, 11, 18, 19, 20]. Special attention was paid to previously unmodeled joints and articulation constraints to achieve physiologically accurate ROM and naturalistic motion patterns during whole-body movements.

The muscular system was developed by rigorously following Gray's Anatomy[1]. The path of each muscle-tendon unit was individually verified and refined to ensure anatomical accuracy in the routes and attachment points. The architectural parameters used in the simulation, including optimal fiber

length, physiological cross-sectional area, pennation angle and tendon slack length were implemented based on existing anatomical studies and validated models [2, 3, 4, 8, 18, 20, 21, 22, 23, 24, 25, 26, 27]. For muscle parameters not included in existing literature, we developed a systematic approach for parameter estimation based on primary anatomical data[28, 29, 30, 31, 32, 33, 34, 35, 36]. The force-generating capability of a muscle-tendon unit was modeled with normalized fiber force-length-velocity relationship[37] and neuromuscular dynamics[38], ensuring physiologically plausible muscle behaviors.

Figure A1 highlights representative muscle-tendon units across various body parts in our model. Together, our SMS-Human model represents a musculoskeletal system with much higher anatomical accuracy than that of existing 3D anatomical databases [10, 39]. The high dimensionality of muscle-tendon units poses both advantages and challenges as a platform for realistic simulation of human movements.

Deep reinforcement learning for sensorimotor control

The high dimensionality of muscle actuation present a fundamental challenge in motor control[40, 41]. In humans, motor control commands are executed through coordinated muscle synergistic activation[42, 43].Inspired by human motor control, we developed a stage-wise hierarchical deep reinforcement learning method to control the SMS-Human model to perform whole-body movement tasks (Fig. A2). We implement muscle grouping based on dynamic similarities and anatomical constraints. Within each muscle group, we implemented a hierarchical control strategy, where muscles received shared group control signals for group-level coordination and individual state-dependent refinements based on sensory feedback and task demands.

During training, observation matrix of multisensory information was delivered to a Soft Actor-Critic[44](SAC)-based controller, which included a hierarchical actor module, an action refinement module and a critic network. The hierarchical actor module contained two networks: the group action network generated actions at the muscle group level, and the unit action network provided state-dependent adjustment weights for individual muscle-tendon units. Following the hierarchical actor, the action refinement module further adjusted the output actions for movement control by applying adjustment weights to group actions. Rewards for reinforcement learning were designed based on whether the model behavior matched the reference data or whether the task goal was achieved, as well as task-specific terms. The network controller was trained through a stage-wise learning strategy that progressively increased task complexity.

Simulation of bipedal walking

The DRL approach was used to train the network controller for simulating natural human bipedal walking by the SMS-Human model. During training, the network controller received kinematic references as well as the sensory signals generated in simulation. The DRL algorithm maximized a reward function that encouraged simulated movements to match the reference motion capture data, while maintaining muscle activations within the physiological range. To promote control efficiency while preserving biomechanical validity, we implemented targeted simplifications by limiting the ROM of non-critical articulations of joints (e.g., finger joints) during walking.

The trained network controller successfully reproduced natural human bipedal walking patterns (Fig. A3a). Quantitative evaluations indicated the high precision in the kinematics and dynamics of the simulated locomotion. First, joint angle trajectories of eight representative joints closely tracked the motion capture data from the human subject throughout three gait cycles of bipedal walking (Fig. A3b). Second, muscle activities in our SMS-Human model during simulated walking could largely match the EMG signals (with some exhibiting time-locked phase shifts) recorded from corresponding muscles of the same reference human subject during his bipedal walking (Fig. A3c).

In Figure A3d, the comprehensive dynamics of joints and muscles is visualized to illustrate the capability of the SMS-Human model to simulate and analyze complex whole-body musculoskeletal coordination. Selective examination of specific components in our model could also help to capture subtle yet important aspects of walking. We predicted physiologically plausible activation patterns for deep, hard-to-measure muscles (e.g., flexor digitorum longus, internal oblique) and subtle spinal movements for torso stability (Fig. A3e). This demonstrates the model's power to detailed dynamics of all human muscles and joints in the absence of complete experimental measurements on humans.

Vision-guided object manipulation

We next examined the ability of the SMS-Human model in simulating a visually guided manipulation task involving picking up an “object" (a bottle) on the table, moving it first to align with the “target" (a virtual bottle) above the table, and then following the target’s random leftward or rightward movement (starting at 0.5 s after task initialization). The coordinates and orientation of the object and target were not explicitly provided to the controller during task execution. The controller therefore must infer the spatial relationship and movement goal through its visual inputs and other sensory feedback.

Binocular images (224×224 pixels, 80° field-of-view) captured by cameras in eyes were pre-processed by a distance-dependent Gaussian filter to simulate foveal visual sensing with peripheral blurring. A pre-trained convolutional neural network was then applied to acquire task-relevant visual representations as inputs for the network controller. The trained network controller successfully performed the bottle pick-up and translocation task in an eye-head-hand coordinated manner (Fig. A4a). Notably, the model exhibited visual tracking behavior with coordinated eye-head movements to fixate around the object. The learned visuomotor control of our model was similar to that of a human subject in performing the same task. The eyes of the subject were elevated to guide the hand movement during bottle pick-up and rotated laterally with the translocating object (Fig. A4b).

Quantitative evaluation indicates that SMS-Human model achieved expected object manipulation towards the target. During the target tracking phase (after 0.5 s), the object stayed close to the target with an average translational difference of 0.15 ± 0.25 cm and a rotational difference of 0.01 ± 0.02 radians, while the average fixation-to-object offset was 0.53 ± 0.43 cm (mean$\pm$SEM, n=10, Fig. A4c). The convergence of position and orientation of the object to the target (Fig. A4d) suggests effective vision-guided motor control, in which the model continuously updated its motor commands based on visual and other sensory feedback. The movement trajectories in Fig. A4e illustrate human-like task-dependent eye-head-hand kinematic patterns. The learned activation patterns of extraocular muscles during object manipulation are shown in Fig. A4f, representing the unique capability of our model to simulate natural control of eye movements. Our model was capable of generating appropriate synergistic muscle activation for object tracking, and this visual tracking was integrated with other sensory signals to coordinate motor behaviors.

Bicycle riding

To demonstrate the capability of our SMS-Human model for simulating human-machine interaction, we designed a bicycling task that requires coordinated control for interaction with a bicycle, which was confined in vertical orientation with movable pedals and wheels for forward movement. During training, the network controller was rewarded for maintaining stable upper body posture while holding the fixed handlebar via sensory feedback signals and for matching the model’s body keypoint trajectories to synthetic 3D trajectories from pre-generated bicycling motion (Fig. A5a).

After training, the model successfully executed rhythmic pedaling movements while maintaining upper body stability, achieving a natural cycling posture. The sequential visualization of the pedaling cycle showed smooth transitions between the top and bottom foot positions characteristic of proper cycling mechanics (Fig. A5b). Quantitative analysis reveals high precision in the control of simulated body movements (Fig. A5c). The temporal profiles of lower limb kinematics demonstrate coordinated cyclical patterns similar to human cycling motion capture[45]. The vertical contact force at the feet showed characteristic peaks during the power phase of each cycle, indicating effective force transmission to the bicycle (Fig. A5d). These results indicate that our model is capable of simulating coordinated whole-body movements while interacting with external devices.

Discussion

Coordinated human movements arise from the intricate integration of multimodal sensation, sensorimotor transformation, and motor execution within a closed-loop system. This work seeks to computationally realize these processes and generate adaptive motor behaviors across various tasks with a comprehensive whole-body sensory-musculoskeletal model. By coupling multisensory inputs with high-dimensional motor outputs through learning-based approaches, our model provides a new platform for investigating the spatiotemporal dynamics of the human musculoskeletal system during motion.

References

[1] S. Standring. *Gray's Anatomy: The Anatomical Basis of Clinical Practice*. Gray's Anatomy Series. Elsevier Limited, 41st edition, 2016.

[2] Katherine R Saul, Xiao Hu, Craig M Goehler, Meghan E Vidt, Melissa Daly, Anca Velisar, and Wendy M Murray. Benchmarking of dynamic simulation predictions in two software platforms using an upper limb musculoskeletal model. *Computer methods in biomechanics and biomedical engineering*, 18(13):1445–1458, 2015.

[3] Daniel C McFarland, Benjamin I Binder-Markey, Jennifer A Nichols, Sarah J Wohlman, Marije De Bruin, and Wendy M Murray. A musculoskeletal model of the hand and wrist capable of simulating functional tasks. *IEEE Transactions on Biomedical Engineering*, 70(5):1424–1435, 2022.

[4] Scott L Delp, J Peter Loan, Melissa G Hoy, Felix E Zajac, Eric L Topp, and Joseph M Rosen. An interactive graphics-based model of the lower extremity to study orthopaedic surgical procedures. *IEEE Transactions on Biomedical engineering*, 37(8):757–767, 1990.

[5] Apoorva Rajagopal, Christopher L Dembia, Matthew S DeMers, Denny D Delp, Jennifer L Hicks, and Scott L Delp. Full-body musculoskeletal model for muscle-driven simulation of human gait. *IEEE Transactions on Biomedical Engineering*, 63(10):2068–2079, 2016.

[6] Adrian KM Lai, Allison S Arnold, and James M Wakeling. Why are antagonist muscles co-activated in my simulation? a musculoskeletal model for analysing human locomotor tasks. *Annals of biomedical engineering*, 45:2762–2774, 2017.

[7] Sung Hee Lee, Eftychios Sifakis, and Demetri Terzopoulos. Comprehensive biomechanical modeling and simulation of the upper body. *ACM Transactions on Graphics (TOG)*, 28(4):1–17, 2009.

[8] Stefan Schmid, Katelyn A Burkhart, Brett T Allaire, Daniel Grindle, and Dennis E Anderson. Musculoskeletal full-body models including a detailed thoracolumbar spine for children and adolescents aged 6–18 years. *Journal of biomechanics*, 102:109305, 2020.

[9] Emanuel Todorov, Tom Erez, and Yuval Tassa. Mujoco: A physics engine for model-based control. In *2012 IEEE/RSJ International Conference on Intelligent Robots and Systems*, pages 5026–5033. IEEE, 2012.

[10] Nobutaka Mitsuhashi, Kaori Fujieda, Takuro Tamura, Shoko Kawamoto, Toshihisa Takagi, and Kousaku Okubo. Bodyparts3d: 3d structure database for anatomical concepts. *Nucleic acids research*, 37(suppl_1):D782–D785, 2009.

[11] Jayishni N Maharaj, Michael J Rainbow, Andrew G Cresswell, Sarah Kessler, Nicolai Konow, Dominic Gehring, and Glen A Lichtwark. Modelling the complexity of the foot and ankle during human locomotion: the development and validation of a multi-segment foot model using biplanar videoradiography. *Computer Methods in Biomechanics and Biomedical Engineering*, 25(5):554–565, 2022.

[12] CJ Nester, AM Liu, E Ward, D Howard, J Cocheba, T Derrick, and P Patterson. In vitro study of foot kinematics using a dynamic walking cadaver model. *Journal of biomechanics*, 40(9):1927–1937, 2007.

[13] Andrea Mapelli, Domenico Galante, Nicola Lovecchio, Chiarella Sforza, and Virgilio F Ferrario. Translation and rotation movements of the mandible during mouth opening and closing. *Clinical Anatomy: The Official Journal of the American Association of Clinical Anatomists and the British Association of Clinical Anatomists*, 22(3):311–318, 2009.

[14] Sean L Borkowski, Eric Tamrazian, Richard E Bowen, Anthony A Scaduto, Edward Ebramzadeh, and Sophia N Sangiorgio. Challenging the conventional standard for thoracic spine range of motion: a systematic review. *Jbjs Reviews*, 4(4):e5, 2016.

[15] Won June Lee, Ji Hong Kim, Yong Un Shin, Sunjin Hwang, and Han Woong Lim. Differences in eye movement range based on age and gaze direction. *Eye*, 33(7):1145–1151, 2019.

[16] Wojciech Piotr Kiebzak, Arkadiusz Łukasz Żurawski, and Michał Kosztołowicz. Alignment of the sternum and sacrum as a marker of sitting body posture in children. *International Journal of Environmental Research and Public Health*, 19(23):16287, 2022.

[17] Keisuke Negishi, Kota Watanabe, Atsushi Teramoto, Kenta Yamatsu, and Mizuho Hayashi. Three-dimensional motion of the toes with simulated contraction of individual toe flexors and extensors: A cadaver study. *The Foot*, 56:102044, 2023.

[18] Miguel Christophy, Nur Adila Faruk Senan, Jeffrey C Lotz, and Oliver M O'Reilly. A musculoskeletal model for the lumbar spine. *Biomechanics and modeling in mechanobiology*, 11:19–34, 2012.

[19] Scott D Uhlrich, Rachel W Jackson, Ajay Seth, Julie A Kolesar, and Scott L Delp. Muscle coordination retraining inspired by musculoskeletal simulations reduces knee contact force. *Scientific reports*, 12(1):9842, 2022.

[20] Jonathan D Mortensen, Anita N Vasavada, and Andrew S Merryweather. The inclusion of hyoid muscles improve moment generating capacity and dynamic simulations in musculoskeletal models of the head and neck. *PloS one*, 13(6):e0199912, 2018.

[21] Thomas L Wickiewicz, Roland R Roy, Perry L Powell, and V Reggie Edgerton. Muscle architecture of the human lower limb. *Clinical Orthopaedics and Related Research*, 179:275–283, 1983.

[22] Melissa G Hoy, Felix E Zajac, and Michael E Gordon. A musculoskeletal model of the human lower extremity: the effect of muscle, tendon, and moment arm on the moment-angle relationship of musculotendon actuators at the hip, knee, and ankle. *Journal of biomechanics*, 23(2):157–169, 1990.

[23] James A Friederich and Richard A Brand. Muscle fiber architecture in the human lower limb. *Journal of biomechanics*, 23(1):91–95, 1990.

[24] Frank C Anderson and Marcus G Pandy. Dynamic optimization of human walking. *J. Biomech. Eng.*, 123(5):381–390, 2001.

[25] Alexander Priamikov, Maria Fronius, Bertram Shi, and Jochen Triesch. Openeyesim: A biomechanical model for simulation of closed-loop visual perception. *Journal of vision*, 16(15):25–25, 2016.

[26] Faes D Kerkhof, Timo van Leeuwen, and Evie E Vereecke. The digital human forearm and hand. *Journal of Anatomy*, 233(5):557–566, 2018.

[27] Ajay Seth, Meilin Dong, Ricardo Matias, and Scott Delp. Muscle contributions to upper-extremity movement and work from a musculoskeletal model of the human shoulder. *Frontiers in neurorobotics*, 13:90, 2019.

[28] TMGJ Van Eijden, JAM Korfage, and P Brugman. Architecture of the human jaw-closing and jaw-opening muscles. *The Anatomical Record: An Official Publication of the American Association of Anatomists*, 248(3):464–474, 1997.

[29] Mary D Klein Breteler, Cornelis W Spoor, and Frans CT Van der Helm. Measuring muscle and joint geometry parameters of a shoulder for modeling purposes. *Journal of biomechanics*, 32(11):1191–1197, 1999.

[30] Scott L Delp, Srikanth Suryanarayanan, Wendy M Murray, Jim Uhlir, and Ronald J Triolo. Architecture of the rectus abdominis, quadratus lumborum, and erector spinae. *Journal of biomechanics*, 34(3):371–375, 2001.

[31] JH Koolstra and TMGJ Van Eijden. Combined finite-element and rigid-body analysis of human jaw joint dynamics. *Journal of biomechanics*, 38(12):2431–2439, 2005.

[32] Melissa R Lachowitzer, Anne Ranes, and Gary T Yamaguchi. Musculotendon parameters and musculoskeletal pathways within the human foot. *Journal of applied biomechanics*, 23(1):20–41, 2007.

[33] Samuel R Ward, Carolyn M Eng, Laura H Smallwood, and Richard L Lieber. Are current measurements of lower extremity muscle architecture accurate? *Clinical orthopaedics and related research*, 467(4):1074–1082, 2009.

[34] Jordi Borst, Patrick A Forbes, Riender Happee, and DirkJan HEJ Veeger. Muscle parameters for musculoskeletal modelling of the human neck. *Clinical biomechanics*, 26(4):343–351, 2011.

[35] Geoffrey G Handsfield, Craig H Meyer, Joseph M Hart, Mark F Abel, and Silvia S Blemker. Relationships of 35 lower limb muscles to height and body mass quantified using mri. *Journal of biomechanics*, 47(3):631–638, 2014.

[36] Mojtaba Mirakhorlo, Judith MA Visser, BAAX Goislard de Monsabert, FCT Van der Helm, Huub Maas, and HEJ Veeger. Anatomical parameters for musculoskeletal modeling of the hand and wrist. *International Biomechanics*, 3(1):40–49, 2016.

[37] Matthew Millard, Thomas Uchida, Ajay Seth, and Scott L Delp. Flexing computational muscle: modeling and simulation of musculotendon dynamics. *Journal of biomechanical engineering*, 135(2):021005, 2013.

[38] Daniel M Wolpert and Zoubin Ghahramani. Computational principles of movement neuroscience. *Nature neuroscience*, 3(11):1212–1217, 2000.

[39] Tracey Wilkinson. Primal pictures anatomy teaching resources: 3d anatomy software and 3d real-time viewer. *Journal of Anatomy*, 220(1):118, 2012.

[40] Nikolai Bernstein. The co-ordination and regulation of movements. *The co-ordination and regulation of movements*, 1966.

[41] Lena H Ting, Stacie A Chvatal, Seyed A Safavynia, and J Lucas McKay. Review and perspective: neuromechanical considerations for predicting muscle activation patterns for movement. *International journal for numerical methods in biomedical engineering*, 28(10):1003–1014, 2012.

[42] Sten Grillner. Neurobiological bases of rhythmic motor acts in vertebrates. *Science*, 228(4696):143–149, 1985.

[43] Nadia Dominici, Yuri P Ivanenko, Germana Cappellini, Andrea d'Avella, Vito Mondì, Marika Cicchese, Adele Fabiano, Tiziana Silei, Ambrogio Di Paolo, Carlo Giannini, et al. Locomotor primitives in newborn babies and their development. *Science*, 334(6058):997–999, 2011.

[44] Tuomas Haarnoja, Aurick Zhou, Pieter Abbeel, and Sergey Levine. Soft actor-critic: Off-policy maximum entropy deep reinforcement learning with a stochastic actor. In *International Conference on Machine Learning*, pages 1861–1870. PMLR, 2018.

[45] Caitlin E Clancy, Anthony A Gatti, Carmichael F Ong, Monica R Maly, and Scott L Delp. Muscle-driven simulations and experimental data of cycling. *Scientific Reports*, 13(1):21534, 2023.

Appendix

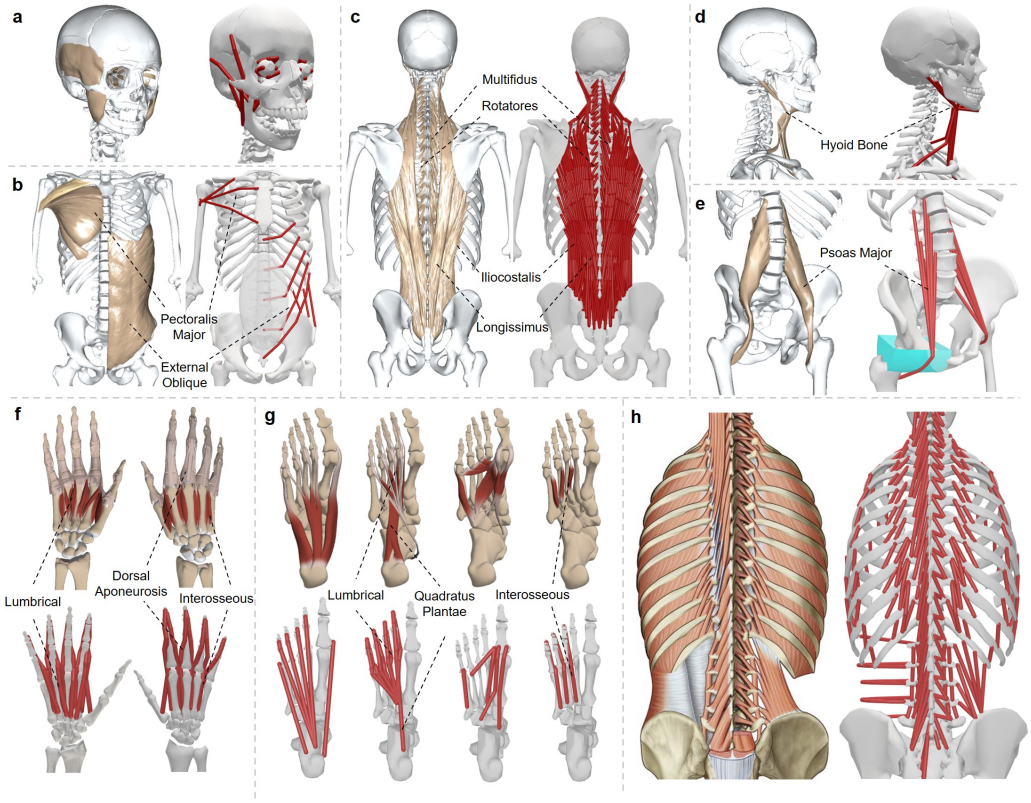

Figure A1: **Anatomically precise reconstruction of muscle-tendon units in the SMS-Human model.** Side-by-side comparisons of the anatomical arrangements of representative muscles and corresponding muscle-tendon units (thick red lines) in the model. In **a-e**, BodyParts3D anatomical database[10] (left) was used for modeling muscle-tendon units (right). In **f-g**, Primal Pictures 3D atlas database[39] (upper) was used for modeling muscle-tendon units (lower). **a**, Head, temporomandibular joint, masticatory and extraocular muscles, and corresponding muscle-tendon units. **b**, Thorax and abdominal region, pectoralis major and external oblique muscles and corresponding muscle-tendon units. **c**, Back region, iliocostalis and longissimus muscles were modeled with multiple muscle-tendon units. Multifidus and rotatores muscles between spinal segments were modeled individually. **d**, Neck, the hyoid bone and the attached suprahyoid/infrahyoid muscle groups and corresponding model units. **e**, Wrapping surfaces (shown in light blue) were added around body segments for constraining the muscle contractile pathways, as illustrated here for the psoas major muscle. **f**, Hand, palmar (left) and dorsal (right) views of the right hand. Lumbrical and interosseous muscles were interconnected to the dorsal aponeurosis, extending to the fingertips and modeled as distinct muscle-tendon units. **g**, Foot, all four layers of intrinsic foot muscles individually modeled as muscle-tendon units. **h**, Detailed back musculature from Gray's Anatomy[1] (left) and the corresponding muscle-tendon units in the model (right).

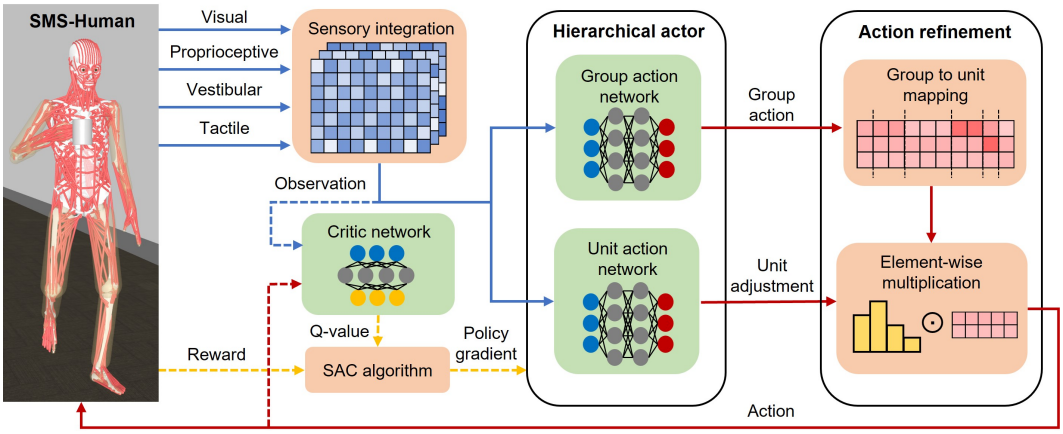

Figure A2: **Schematic illustration of the hierarchical deep reinforcement learning for high-dimensional sensorimotor control.** Visual features and values from proprioceptive, vestibular and tactile sensors were integrated to form the observation matrix. The observation was then processed by a SAC-based controller including a critic network, and a hierarchical actor module followed by an action refinement module. The hierarchical actor module consisted of a high-level group action network generating shared actions for each muscle group, and a low-level unit action network producing state-dependent adjustment weights for each individual muscle-tendon unit. The action refinement module adjusted output actions at unit-level via group-unit mapping and element-wise multiplication of group actions and unit adjustment weights. The critic updated the estimation of Q-values, informing policy improvement.

Sensation	Observation (policy input)	Unit	Dimension
Visual	RGB image of left eye camera	pixel	(224,224,3)
	RGB image of right eye camera	pixel	(224,224,3)
Proprioceptive	Joint angles	rad	278
	Joint velocities	rad/s	278
	Joint acceleration	rad/s^2	278
	Muscle length	m	1266
	Muscle velocity	m/s	1266
	Muscle activation	unitless	1266
	Muscle force	N	1266
Vestibular	Velocity	cm/s	3
	Acceleration	cm/s^2	3
	Angular velocity	rad/s	3
Tactile	Contact force	N	78

Table A1: Multisensory observations of SMS-Human model.

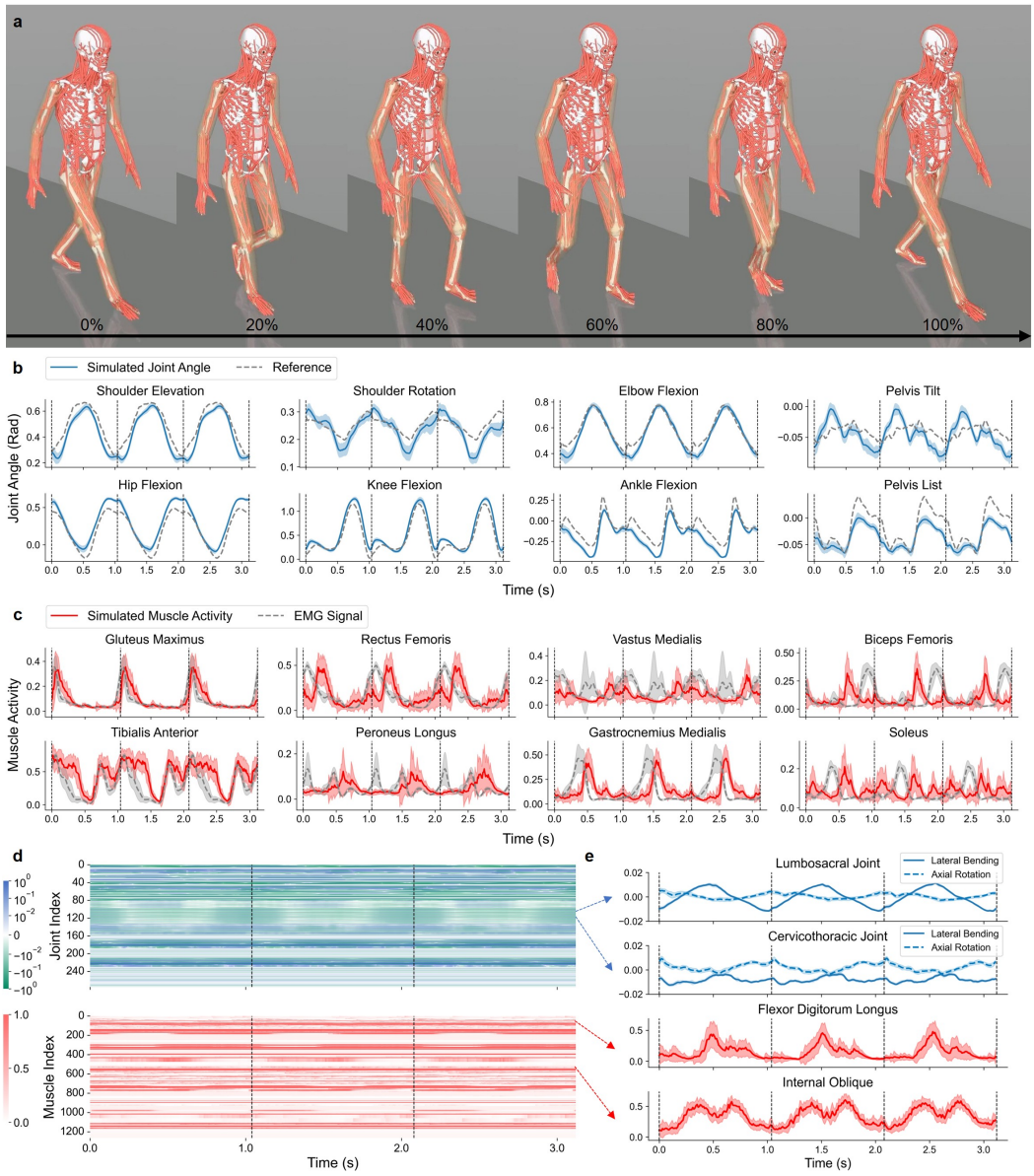

Figure A3: **Whole-body simulation for bipedal locomotion**. **a**, Simulated bipedal locomotion sequence demonstrating a full gait cycle during straight walking. **b**, Comparison of SMS-Human-simulated (blue lines) and reference (gray dashed lines) joint angle trajectories for eight representative upper and lower body joints during walking, for three gait cycles. Pelvis tilt is the rotation around the lateral axis, and pelvis list is the rotation around the anteroposterior axis, both relative to the ground. **c**, Simulated muscle activity patterns (red lines) and experimental EMG signals (gray dashed lines) for eight major lower limb muscles during walking, for three gait cycles. **d**, Comprehensive joint kinematics and muscle activations during the three gait cycles of bipedal walking. Upper panel: temporal changes of joint angles (in radian) in an example walking trial; lower panel: simulated muscle activity profiles in the same walking trial. **e**, Selected examples of simulated joint angle and muscle activity during bipedal walking. Upper panel: lateral bending/axial rotation of two spinal joints showing subtle movements, indicating stable torso control during walking; lower panel: activity patterns of two deep muscles, which could not be readily measured experimentally. In **b-e**, vertical black dash lines denote the time of right heel strike; shaded regions denote one standard deviation (n=30 for simulated joint angles and muscle activities, n=7 for EMG).

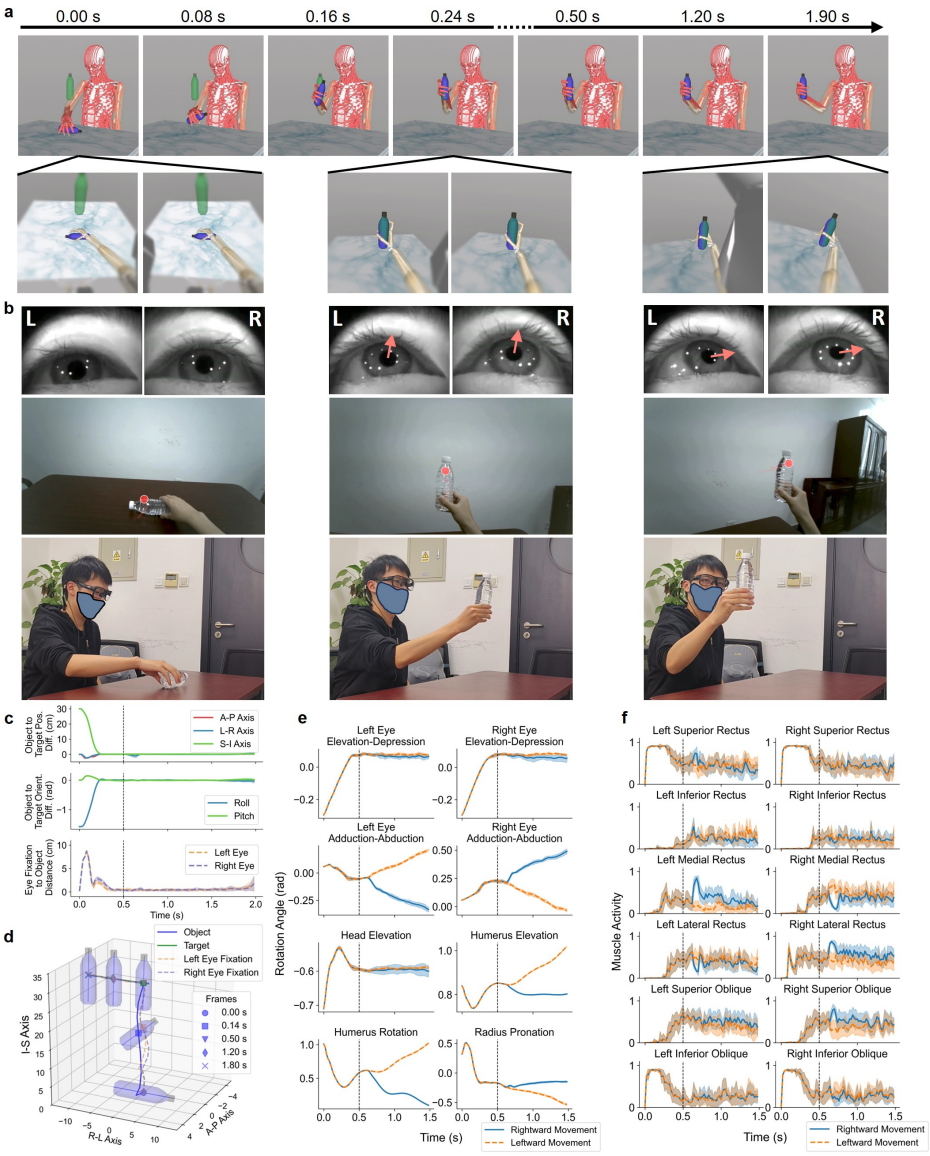

Figure A4: **Visuomotor coordination in the object manipulation task. a**, Top: Simulated model behavior showing picking-up, holding, and translocating the object (blue bottle) in accordance to the target cue (semitransparent green bottle). The object and the target cue largely overlapped after 0.24 s. Bottom: Visual inputs to the model at three time points during the task. **b**, The same task performed by a representative human subject, showing the eye-head-hand coordination at three key time points during the task. Top panels: human eye movement directions. Red arrows, the combined eye rotation directions. Middle panels: human visual scenes and fixation points. Bottom panels: human behavior recorded from a camera in the environment. **c**, Spatial differences between the object and target, and between the eye fixation point and object. Zero value indicates exact alignment. Top panel: position differences between centers of the object and target. Orthogonal coordinate axes of the model: A-P, anterior-posterior; L-R, left-right; S-I, superior-inferior. Middle panel: orientation differences between the object and target, measured in two angular axes. Bottom panel: distance between the eye fixation points and the object. **d**, 3D trajectories (in cm) during target tracking of the rightward-moving task, with the object's initial position at the origin of coordinates. **e,f**, Angular kinematics of eye rotations, head and upper limb articulations (**e**), and activation of bilateral extraocular muscles (**f**) in our model during object manipulation task, for leftward (orange) and rightward (blue) movements. In **c-f**, shaded regions denote one standard deviation across 10 trials; vertical black dashed lines denote target movement onset time; A-P, anterior-posterior; L-R, left-right; S-I, superior-inferior.

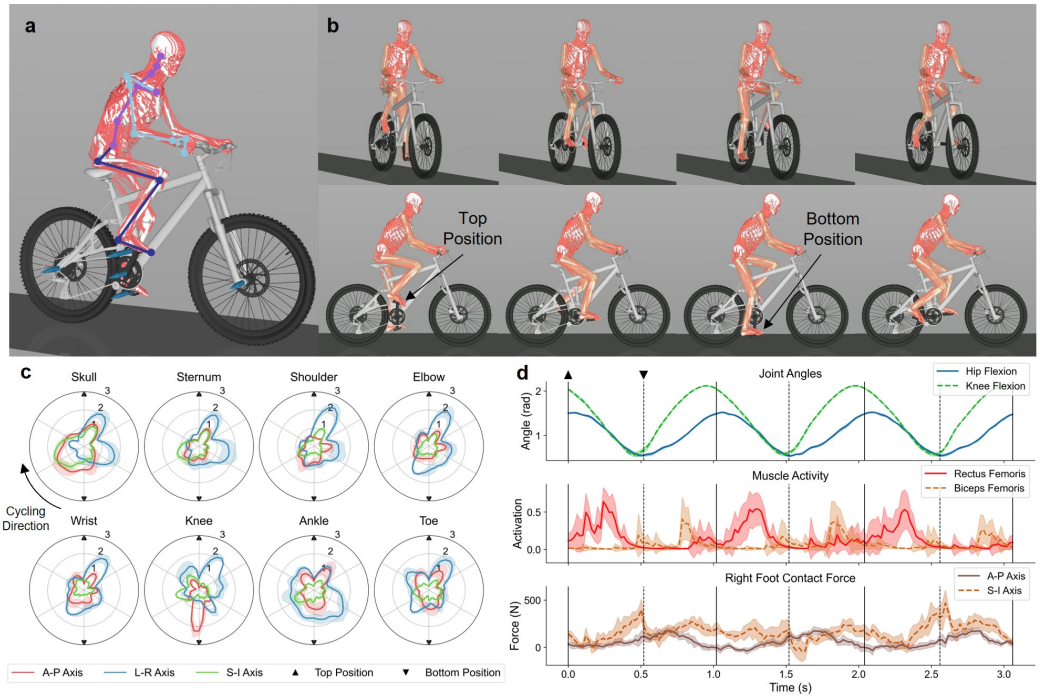

Figure A5: **Whole-body simulation for bicycling. a**, Simulation of a bicycling task by the SMS-Human model, with body keypoints of the right side illustrated in different colors for different body parts (body keypoints of the left side are not shown for visualization clarity). The network controller was rewarded for matching the motion trajectories of these keypoints to the synthetic reference trajectories during training. The blue arrows represent the rotation axes of the crankset, pedals, and wheels of the bicycle. **b**, Sequential visualization of the pedaling cycle of learned model behavior. Top and bottom positions are marked for the right foot. **c**, Spatial deviations (in cm) of representative body keypoints to their reference positions (with 0 value indicating exact matching), in each pedaling cycle during task execution after training, along three axes of the environment. **d**, Temporal patterns of lower limb kinematics and dynamics during cycling, including representative joint angles (top panel), activation of muscles (middle panel) and contact force between right foot and the pedal (bottom panel). Black solid and dashed lines indicate the top and bottom positions of the right foot respectively. In **c-d**, shaded regions denote one standard deviation across 10 trials; A-P, anterior-posterior; L-R, left-right; S-I, superior-inferior.